

# Diagrammatic Monte Carlo for Fermionic Rényi Entanglement Entropy

Boyuan Shi<sup>1</sup>

<sup>1</sup>*Department of Physics, Imperial College London, London SW7 2AZ, United Kingdom*

We develop a direct diagrammatic Monte Carlo framework for the Rényi entanglement entropy of interacting lattice fermions. The method starts from the fermionic graded-swap representation of  $Z_n[A] = \text{Tr}_A \rho_A^n$ , which converts the entropy problem into a replicated path integral with mixed temporal boundary conditions on the entangling region. In this representation the replica momenta are half-shifted,  $q_m = (2m+1)\pi/n$ , and the interaction expansion has a determinant form suitable for connected-determinant summation. We combine this expansion with a many-configuration Markov-chain Monte Carlo sampler to obtain order-by-order corrections for very large systems to very high orders. As a benchmark, we compare the order-by-order coefficients of a  $3 \times 3$  Hubbard cluster with exact diagonalization. We then report a production calculation for a  $40 \times 40$  periodic lattice with a square subregions. The dominant system-size limitation is therefore memory rather than a conventional auxiliary-field sign problem. The results provide a step toward diagrammatic calculations of fermionic entanglement observables in regimes where direct quantum Monte Carlo sampling is costly or sign-problem limited.

## I. INTRODUCTION

Entanglement entropy has become one of the most useful diagnostics of quantum many-body structure. It obeys an area law in many gapped local systems, while fermions with a Fermi surface show logarithmic violations tied to the Fermi surface geometry [1–4]. Computing this quantity for interacting fermions is still difficult. Quantum Monte Carlo can access large sign-free systems [5], and replica, swap-operator, continuous-time, determinantal, and auxiliary-field approaches have made Rényi entropy calculations practical in many spin, bosonic, and fermionic settings [6–10]. Recent high-precision algorithms have further pushed QMC access to universal entanglement terms in two dimensions and to interacting fermion models [11–16]. Nevertheless, finite-temperature, two-dimensional, sign-problematic fermionic regimes remain hard to reach.

Diagrammatic Monte Carlo provides a complementary route. Instead of sampling many-body configurations in the original Hilbert space, it samples terms in a Feynman expansion and can reach high perturbative orders directly in the thermodynamic limit or at large finite size. It has been applied to correlated fermions, BCS regimes, pseudogap physics in the doped two-dimensional Hubbard model, and magnetic transitions in the three-dimensional Hubbard model [17–24]. Connected-determinant and related high-order sampling schemes exploit cancellations between diagram topologies and make it inexpensive to measure many related configurations [25–27].

Most diagrammatic calculations have focused on thermodynamic quantities, self-energies, or correlation functions. Entanglement is different because the observable changes the temporal topology of the path integral and depends on the geometry of the chosen subregion. In a perturbative formulation this means that the usual connected expansion has to be reorganized around replica boundary conditions, rather than around a local operator inserted in an otherwise ordinary partition function. A related perturbative approach expresses the entropy

through connected correlation functions in the ordinary field theory [28]. Here we instead work directly on the replicated manifold generated by the fermionic swap operator and construct a connected-determinant expansion of  $\ln Z_2[A]$ , keeping the finite spatial region  $A$  explicit throughout. This keeps the method close to existing high-order diagrammatic machinery while avoiding a separate reconstruction of the entropy from many correlation functions.

The resulting coefficients can be checked order by order against exact diagonalization before moving to larger systems, so the calculation below serves as a controlled benchmark for the method.

The motivation is also experimental: two-copy interference, quantum gas microscopy, and randomized measurements provide routes to Rényi entropies in cold-atom Hubbard and spin systems [29–31]. These developments make it useful to have controlled theoretical benchmarks for finite regions in fermionic lattice models, including regimes where direct configuration-space sampling is costly. This paper develops the formulation, derives the graded-swap Green functions and determinant expansion, summarizes the sampler, and benchmarks the order-by-order coefficients against exact diagonalization before presenting a  $40 \times 40$  production run.

## II. MODEL AND OBSERVABLE

We study the repulsive Hubbard model on an  $N_1 \times N_2$  square lattice with periodic boundary conditions and nearest-neighbor hopping  $t = 1$ ,

$$H = - \sum_{\langle ij \rangle, \sigma} c_{i\sigma}^\dagger c_{j\sigma} + U \sum_i n_{i\uparrow} n_{i\downarrow} - \mu \sum_{i,\sigma} n_{i\sigma}. \quad (1)$$

The thermal density matrix is  $\rho = e^{-\beta H}/Z_1$ , with  $Z_1 = \text{Tr} e^{-\beta H}$ . For a spatial region  $A$ , the second Rényi partition function and entropy are

$$Z_2[A] = \text{Tr}_A \rho_A^2, \quad S_2[A] = - \ln Z_2[A], \quad (2)$$

where  $\rho_A = \text{Tr}_{\bar{A}} \rho$ . In the numerical sections we report coefficients of the intensive logarithm

$$f_A(\xi) = \frac{1}{N} \ln Z_2[A; \xi], \quad N = N_1 N_2, \quad (3)$$

so that  $S_2[A]/N = -f_A(1)$ . The perturbative parameter  $\xi$  is defined through a shifted homotopy Hamiltonian below. The quantities denoted ‘‘order  $k$ ’’ in the numerical results are the coefficients  $c_k/N$  in

$$f_A(\xi) = f_A^{(0)} + \sum_{k \geq 1} \frac{c_k}{N} \xi^k. \quad (4)$$

The noninteracting term  $f_A^{(0)}$  is evaluated deterministically from the free correlation matrix; the Monte Carlo calculation targets the interaction corrections.

For an origin-square region on a periodic lattice we use the convention

$$A_r = \{(x, y) : x < r \text{ or } x \geq N_1 - r, \quad y < r \text{ or } y \geq N_2 - r\}. \quad (5)$$

Thus  $r = 8$  on a  $40 \times 40$  lattice corresponds to a periodic square of side 16 and  $|A| = 256$ .

### III. FERMIONIC GRADED-SWAP PATH INTEGRAL

The replica construction is most transparent if one first distinguishes the normalized object  $Z_n[A]$  from the unnormalized twisted trace,

$$\tilde{Z}_n[A] = \text{Tr}_{\mathcal{H}^{\otimes n}} \left[ S_A^{\text{gr}} (e^{-\beta H})^{\otimes n} \right], \quad Z_n[A] = \frac{\tilde{Z}_n[A]}{Z_1^n}. \quad (6)$$

Here  $S_A^{\text{gr}}$  is the fermionic graded cyclic permutation on the subsystem  $A$ . On homogeneous basis states it acts as

$$S_A^{\text{gr}} |a_1, b_1; \dots; a_n, b_n\rangle = (-1)^{p(a_1) \sum_{\beta=2}^n p(a_\beta)} \times |a_2, b_1; \dots; a_1, b_n\rangle, \quad (7)$$

where  $p(a)$  is the fermion parity of the  $A$ -state. The Koszul sign in Eq. (7) is essential: replacing it by a bosonic cyclic permutation gives the wrong phases already in the free theory.

The corresponding coherent-state path integral is

$$\tilde{Z}_n[A] = \int_{\text{gr } A} \mathcal{D}[\bar{c}, c] e^{-S_n[\bar{c}, c]}, \quad (8)$$

where the subscript indicates the graded temporal gluing described below. For the Hubbard model,

$$S_n = \sum_{\alpha=1}^n \int_0^\beta d\tau \left[ \sum_{ij, \sigma} \bar{c}_{i\sigma}^{(\alpha)} (\delta_{ij} \partial_\tau + h_{ij}) c_{j\sigma}^{(\alpha)} + U \sum_i \bar{c}_{i\uparrow}^{(\alpha)} c_{i\uparrow}^{(\alpha)} \bar{c}_{i\downarrow}^{(\alpha)} c_{i\downarrow}^{(\alpha)} \right], \quad (9)$$

with  $h_{ij} = -t_{ij} - \mu \delta_{ij}$ . The action is local in replica index; all information about the entangling cut is carried by the boundary conditions. On the complement  $B$  the fields have the usual anti-periodic condition on each sheet,

$$c_{B\sigma}^{(\alpha)}(\beta^-) = -c_{B\sigma}^{(\alpha)}(0^+), \quad (10)$$

whereas on  $A$  they are cyclically glued through the graded swap,

$$\begin{aligned} c_{A\sigma}^{(\alpha)}(\beta^-) &= c_{A\sigma}^{(\alpha+1)}(0^+), & \alpha < n, \\ c_{A\sigma}^{(n)}(\beta^-) &= -c_{A\sigma}^{(1)}(0^+). \end{aligned} \quad (11)$$

The final minus sign is the coherent-state remnant of the fermionic grading. It is this sign, rather than a detail of convention, that shifts the allowed replica momenta by half a spacing.

Let  $P_A$  and  $P_B$  be one-particle projectors onto the sub-region and its complement. In vector notation the mixed boundary condition is

$$\Psi(\beta^-) = [-P_B \otimes \mathbf{1}_n + P_A \otimes K_n] \Psi(0^+), \quad (12)$$

where  $K_n$  is the graded cyclic shift satisfying  $K_n^n = -\mathbf{1}_n$ . Its eigenvalues are

$$\lambda_m = e^{iq_m}, \quad q_m = \frac{(2m+1)\pi}{n}, \quad m = 0, \dots, n-1. \quad (13)$$

In a replica Fourier sector the boundary condition becomes

$$\psi^{(m)}(\beta^-) = -\Omega_m \psi^{(m)}(0^+), \quad \Omega_m = P_B - e^{iq_m} P_A. \quad (14)$$

We define the free Green function without the conventional extra minus sign,

$$\bar{G}^{(m)}(\tau, \tau') = \langle T_\tau c(\tau) c^\dagger(\tau') \rangle_{0, m}. \quad (15)$$

For a one-particle Hamiltonian  $\mathbf{h}$ , it satisfies

$$(\partial_\tau + \mathbf{h}) \bar{G}^{(m)}(\tau, \tau') = \delta(\tau - \tau') \mathbf{I}, \quad (16)$$

with the boundary condition in Eq. (14). Defining

$$A_m = [\mathbf{I} + \Omega_m^{-1} e^{-\beta \mathbf{h}}]^{-1}, \quad (17)$$

one obtains the exact sector Green function

$$\bar{G}^{(m)}(\tau, \tau') = \begin{cases} e^{-\tau \mathbf{h}} A_m e^{\tau' \mathbf{h}}, & \tau > \tau', \\ e^{-\tau \mathbf{h}} (A_m - \mathbf{I}) e^{\tau' \mathbf{h}}, & \tau < \tau'. \end{cases} \quad (18)$$

The full replicated Green function is reconstructed as

$$\bar{G}_{\alpha\beta}^{(n)}(i, \tau; j, \tau') = \frac{1}{n} \sum_{m=0}^{n-1} e^{iq_m(\alpha-\beta)} \bar{G}^{(m)}(i, \tau; j, \tau'). \quad (19)$$

#### IV. DETERMINANT EXPANSION

The interaction is diagonal in replica space,

$$H_{\text{int}}^{(n)} = U \sum_{\alpha=1}^n \sum_i n_{i\uparrow}^{(\alpha)} n_{i\downarrow}^{(\alpha)}. \quad (20)$$

Let  $X_\ell = (i_\ell, \tau_\ell, \alpha_\ell)$  and  $\mathbf{X} = (X_1, \dots, X_k)$ . The spin- $\sigma$  determinant attached to a set of vertices is

$$D_{\sigma,k}^{(n)}(\mathbf{X}) = \det \left[ \bar{G}_\sigma^{(n)}(X_p, X_q) \right]_{p,q=1}^k. \quad (21)$$

At order  $k$ , Wick's theorem then gives

$$\begin{aligned} \frac{\tilde{Z}_n^{(k)}[A]}{\tilde{Z}_{0,n}[A]} &= \frac{(-U)^k}{k!} \sum_{\{i_\ell, \alpha_\ell\}} \int_0^\beta \prod_{\ell=1}^k d\tau_\ell \\ &\times D_{\uparrow,k}^{(n)}(\mathbf{X}) D_{\downarrow,k}^{(n)}(\mathbf{X}). \end{aligned} \quad (22)$$

All dependence on the entangling region enters through the replica Green functions in Eq. (21); the interaction vertices themselves remain local in space, time, and replica index. The connected part of this expansion gives  $\ln \tilde{Z}_n[A]$ . The normalized entropy object then requires the subtraction

$$\ln Z_n[A] = \ln \tilde{Z}_n[A] - n \ln Z_1. \quad (23)$$

The implementation uses a shifted homotopy Hamiltonian, and therefore shifts the diagonal Green function in the opposite spin channel.

For fixed vertices the code computes the connected determinant coefficients by subset recursions. This is the same organizing principle as connected determinant diagrammatic Monte Carlo [25], but applied to the replica Green functions of Eq. (19).

#### V. MANY-CONFIGURATION MARKOV-CHAIN SAMPLING

To estimate several perturbation orders in one run we use the many-configuration Markov-chain Monte Carlo idea of Ref. 26. An envelope configuration  $V = (X_1, \dots, X_N)$  contains  $N$  vertices. All subsets  $S \subseteq [N]$  with  $|S| \in \mathcal{U}$  are visible at the same Monte Carlo step. For an order-dependent guiding parameter  $\lambda_u > 0$ , define a signed flux

$$\Phi_S(V) = \lambda_{|S|} C_{|S|}(V_S) Q_{\bar{S}|S}(V_{\bar{S}}|V_S), \quad (24)$$

where  $C_u$  is the connected-determinant integrand and  $Q$  is the conditional proposal density for regenerating the complement. The local absolute heat-bath normalization is

$$W(V) = \sum_{\substack{S \subseteq [N] \\ |S| \in \mathcal{U}}} \frac{|\Phi_S(V)|}{\binom{N}{|S|}}. \quad (25)$$

The next retained subset is chosen with probability

$$p(S|V) = \frac{|\Phi_S(V)| / \binom{N}{|S|}}{W(V)}. \quad (26)$$

All subsets are measured, not only the selected subset. The de- $\lambda$  signal for order  $u$  is

$$A_u(V) = \frac{1}{\binom{N}{u}} \sum_{|S|=u} \frac{1}{\lambda_u} \frac{\Phi_S(V)}{W(V)}. \quad (27)$$

Since the chain has stationary density proportional to  $W(V)$ , the common unknown normalization cancels in ratios  $I_u/I_r$ . In the present runs we use learned histogram for each direction as factorized seeds, with envelope order  $N = 9$ .

#### VI. NUMERICAL RESULTS

The benchmark system is a  $3 \times 3$  periodic lattice with  $U = 4$ ,  $\mu = 1$ ,  $\beta = 6$ ,  $\alpha_\uparrow = \alpha_\downarrow = 1.7$ , and  $A$  equal to the first row. We used Chebyshev degree  $25 \times 25$ . The production length was  $4 \times 10^8$  MCMCMC steps over 128 chains after a  $2 \times 10^7$ -step warmup. Figure 1 compares the order-by-order CDet coefficients with exact-diagonalization finite-difference derivatives. First three exact-diagonalization derivatives are stable under varying the finite-difference step  $h$ , giving approximately  $-0.02208008$ ,  $0.026579$ , and  $0.035394$ . The corresponding CDet estimates are  $-0.02208008$ ,  $0.026584(21)$ , and  $0.0353933(69)$ . The agreement is tight within Monte Carlo uncertainties.

We next consider a  $40 \times 40$  periodic lattice with  $U = 3$ ,  $\mu = 1$ ,  $\beta = 8$ ,  $\alpha_\uparrow = \alpha_\downarrow = 1.3$ , and an origin-square subregion with radius  $r = 8$ , i.e.  $|A| = 256$ . The Chebyshev degree is again  $25 \times 25$ . The reference run used  $2 \times 10^8$  production steps over 128 chains. The order-by-order coefficients are shown in Fig. 1.

#### VII. DISCUSSION AND OUTLOOK

The benchmark and production run demonstrate that the graded-swap replica formulation can be coupled directly to connected-determinant sampling. The approach is finite-size oriented: the subregion  $A$ , the lattice size, and the thermal boundary conditions are all built into the free replica Green functions, and the Monte Carlo samples only interaction vertices. This separates the geometric part of the entanglement problem from the stochastic sampling of the interaction expansion. Physically, this is useful because changes in the subregion shape, temperature, or filling enter through the replica propagators, while the connected-determinant machinery continues to measure the same order-by-order entropy object. The method therefore provides a route toward large-scale numerical studies of fermionic entanglement

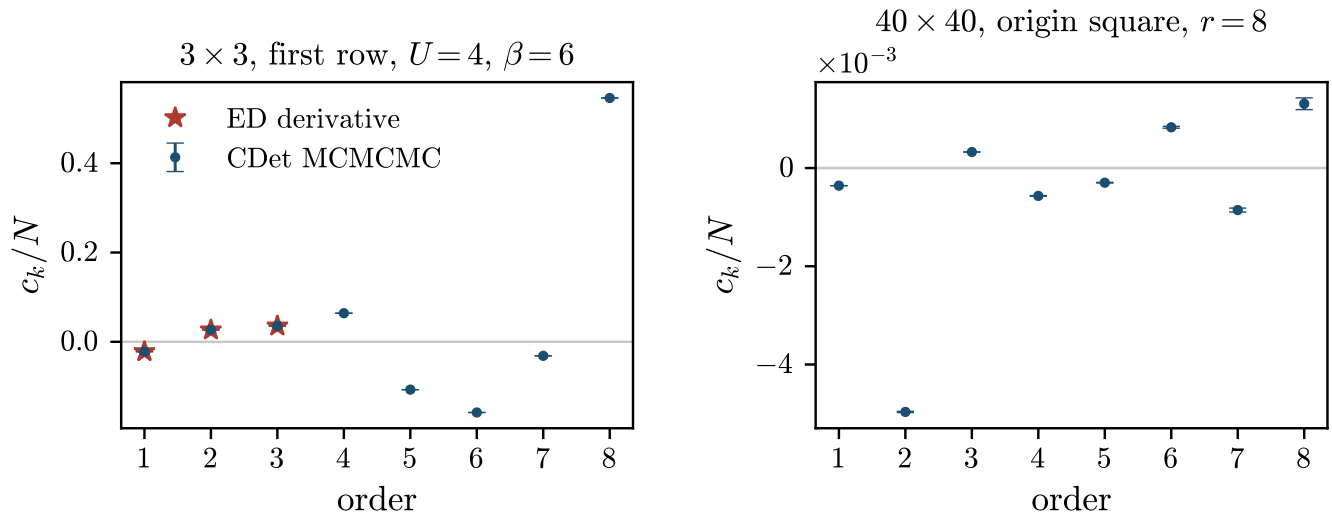


FIG. 1. Order-by-order interaction corrections. Left:  $3 \times 3$  benchmark with ED derivatives, shown as red stars, for the first three coefficients. Right:  $40 \times 40$  production run for a periodic origin-square subregion with radius  $r = 8$ . The plotted values are coefficients of  $\ln Z_2[A]/N$ , not cumulative sums; the omitted zeroth-order terms are the free-system values  $-0.27507894$  (left) and  $-0.04089329$  (right).

in regimes where configuration-space sampling is costly or sign-problem limited.

The main computational pressure is memory. Large lattices and finite subregions require many replica Green-function values, and keeping all precomputed interpolation data resident quickly becomes expensive. In the implementation used here this is controlled by chunked table construction and an LRU cache for Green-function table blocks: frequently reused blocks stay in memory, while cold blocks are evicted and rebuilt or reloaded only when needed. This makes the peak memory footprint a tunable parameter rather than a fixed cost set by the full lattice, subregion, and interpolation grid. The benchmark shown here is therefore best viewed as a proof

that the replica formulation, connected-determinant expansion, and cache-based data layout can be combined in a single workflow. With this infrastructure, the natural physics targets are the temperature, doping, and subregion-size dependence of the Rényi entropy, especially near pseudogap and magnetic regimes where entanglement can provide information complementary to single-particle and thermodynamic observables.

## ACKNOWLEDGMENTS

Numerical calculations were performed on Imperial College Research Computing Service resources.

- 
- [1] J. Eisert, M. Cramer, and M. B. Plenio, *Rev. Mod. Phys.* **82**, 277 (2010).
- [2] M. M. Wolf, *Phys. Rev. Lett.* **96**, 010404 (2006).
- [3] D. Gioev and I. Klich, *Phys. Rev. Lett.* **96**, 100503 (2006).
- [4] B. Swingle, *Phys. Rev. Lett.* **105**, 050502 (2010).
- [5] M. Troyer and U.-J. Wiese, *Phys. Rev. Lett.* **94**, 170201 (2005).
- [6] M. B. Hastings, I. Gonzalez, A. B. Kallin, and R. G. Melko, *Phys. Rev. Lett.* **104**, 157201 (2010).
- [7] S. Humeniuk and T. Roscilde, *Phys. Rev. B* **86**, 235116 (2012).
- [8] T. Grover, *Phys. Rev. Lett.* **111**, 130402 (2013).
- [9] L. Wang and M. Troyer, *Phys. Rev. Lett.* **113**, 110401 (2014).
- [10] P. Broecker and S. Trebst, *J. Stat. Mech.* **2014**, P08015 (2014).
- [11] J. Zhao, Y.-C. Wang, Z. Yan, M. Cheng, and Z. Y. Meng, *Phys. Rev. Lett.* **128**, 010601 (2022).
- [12] J. Zhao, B.-B. Chen, Y.-C. Wang, Z. Yan, M. Cheng, and Z. Y. Meng, *npj Quantum Mater.* **7**, 69 (2022).
- [13] G. Pan, Y. D. Liao, W. Jiang, J. D’Emidio, Y. Qi, and Z. Y. Meng, *Phys. Rev. B* **108**, L081123 (2023).
- [14] J. D’Emidio, R. Orús, N. Laflorencie, and F. de Juan, *Phys. Rev. Lett.* **132**, 076502 (2024).
- [15] W. Jiang, G. Pan, Z. Wang, B.-B. Mao, H. Shen, and Z. Yan, arXiv:2409.20009 10.48550/arXiv.2409.20009 (2025), arXiv:2409.20009.
- [16] Z. Wang, Z. Wang, Y.-M. Ding, B.-B. Mao, and Z. Yan, *Nat. Commun.* **16**, 5880 (2025).
- [17] E. Kozik, K. Van Houcke, E. Gull, L. Pollet, N. Prokof’ev, B. Svistunov, and M. Troyer, *EPL* **90**, 10004 (2010).
- [18] Y. Deng, E. Kozik, N. V. Prokof’ev, and B. V. Svistunov,

- EPL **110**, 57001 (2015).
- [19] W. Wu, M. Ferrero, A. Georges, and E. Kozik, *Phys. Rev. B* **96**, 041105 (2017).
- [20] W. Wu, M. S. Scheurer, S. Chatterjee, S. Sachdev, A. Georges, and M. Ferrero, *Phys. Rev. X* **8**, 021048 (2018).
- [21] F. Šimkovic, R. Rossi, A. Georges, and M. Ferrero, *Science* **385**, eade9194 (2024).
- [22] E. Kozik, E. Burovski, V. W. Scarola, and M. Troyer, *Phys. Rev. B* **87**, 205102 (2013).
- [23] R. Garioud, F. Šimkovic, R. Rossi, G. Spada, T. Schäfer, F. Werner, and M. Ferrero, *Phys. Rev. Lett.* **132**, 246505 (2024).
- [24] C. Lenihan, A. J. Kim, F. Šimkovic, and E. Kozik, *Phys. Rev. Lett.* **129**, 107202 (2022).
- [25] R. Rossi, *Phys. Rev. Lett.* **119**, 045701 (2017).
- [26] F. Šimkovic and R. Rossi, arXiv:2102.05613 10.48550/arXiv.2102.05613 (2021), arXiv:2102.05613.
- [27] B. Shi, arXiv:2507.12349 10.48550/arXiv.2507.12349 (2025), arXiv:2507.12349.
- [28] S. Moitra and R. Sensarma, *Phys. Rev. B* **108**, 174309 (2023).
- [29] R. Islam, R. Ma, P. M. Preiss, M. E. Tai, A. Lukin, M. Rispoli, and M. Greiner, *Nature* **528**, 77 (2015).
- [30] H. Pichler, L. Bonnes, A. J. Daley, A. M. Laeuchli, and P. Zoller, *New J. Phys.* **15**, 063003 (2013).
- [31] A. Elben, B. Vermersch, M. Dalmonte, J. I. Cirac, and P. Zoller, *Phys. Rev. Lett.* **120**, 050406 (2018).